International Journal of Material Forming (2026) 19:26
https://doi.org/10.1007/s12289-026-01991-2

RESEARCH

Machine learning prediction of the forming limit curve of dual phase steels

André Rosiak[1] · Peterson Duarte Diehl[1] · Roderval Marcelino[2] · Lirio Schaeffer[1]

Received: 25 November 2025 / Accepted: 13 February 2026

Abstract
Accurate prediction of the Forming Limit Curve (FLC) is essential for the design of sheet metal stamping processes; however, its experimental determination is costly and limited by data availability. This work investigates the use of Machine Learning techniques to predict the FLC of Dual Phase (DP) steels based on mechanical properties obtained from uniaxial tensile tests. To overcome the scarcity of experimental data, a synthetic database was developed based on statistical consistency and physical constraints, using Kernel Density Estimation, PCA projections, and controlled probabilistic interpolation, followed by the application of physicometallurgical plausibility criteria. The models use physics-based descriptors as input variables, which reflect known metallurgical mechanisms associated with plastic instability, without explicitly incorporating differential equations into the training process. The results show that all models were able to reproduce the characteristic geometry of the FLC, with errors on the order of 10^{-3}–10^{-2}. Among the investigated techniques, Random Forest exhibited the best performance (MAE = 0.0052; MSE = 0.00011; $R^2 = 0.943$), followed by XGBoost, while the Neural Network showed greater variability and a tendency toward overfitting. The results demonstrate that the combination of physics-based descriptors, statistically validated synthetic expansion, and ensemble machine learning methods constitutes a robust and efficient strategy for modeling FLCs of DP steels.

Keywords Dual-phase steels · Forming limit curve · Artificial intelligence

Introduction

The growing demands for improved vehicle safety and energy efficiency have driven the automotive industry toward significant technological advances in recent decades. Among these innovations, Advanced High Strength Steels (AHSS) stand out, as their application enables vehicle mass reduction while enhancing structural performance during crash events [1]. Dual Phase (DP) steels represent the most widely used class of AHSS due to their characteristic microstructure—martensite islands dispersed in a ferritic matrix—which provides a favorable combination of mechanical strength and ductility [2].

The mechanical behavior of DP steels is highly dependent on their microstructural features. In addition to the volume fraction of phases, parameters such as the size, morphology, and spatial distribution of martensitic constituents directly influence the evolution of plastic deformation, strain-hardening capability, and the resistance to damage initiation and propagation [3–6]. Variations in these characteristics, resulting from specific thermomechanical processing conditions, may lead to significant differences in formability among materials belonging to the same strength class—whether between different suppliers, among production batches, or even along a single coil. These aspects highlight the need for rigorous control and accurate assessment of formability, ensuring reproducible performance in automotive stamping operations.

Formability limits are typically determined using the Forming Limit Diagram (FLD), which establishes the boundaries of safe deformation as a function of the major (ε_1) and minor (ε_2) principal strains. Based on a series of mechanical tests conducted under different loading paths, the strain states immediately preceding failure are identified, and their

✉ André Rosiak
andre.rosiak@ufrgs.br

[1] Metal Forming Innovation Center (CBCM), Federal University of Rio Grande do Sul, Porto Alegre, Brazil

[2] Federal University of Santa Catarina, Araranguá, Brazil

Published online: 11 March 2026

interpolation yields the material-specific Forming Limit Curve (FLC) [7–9]. Strain combinations located below the FLC indicate safe deformation conditions, whereas states above it signal a tendency toward plastic instability, localized necking, and eventual fracture.

Although the FLC is widely used and essential for stamping process design, its experimental determination requires considerable time, specialized equipment, and a large number of tests. In this context, alternatives capable of reducing the experimental burden while maintaining high predictive reliability are of significant scientific and industrial interest.

Artificial Intelligence (AI) has emerged as a powerful tool for predicting physical and operational states in complex systems, particularly in industrial and scientific processes characterized by multiple interdependent variables and nonlinear behavior. This ability to capture complex relationships has driven research efforts aimed at applying AI techniques to the prediction of Forming Limit Curves (FLCs) [10–17].

Artificial Neural Networks (ANNs) were employed in [15] to predict the FLCs of Ti6Al4V and Al6061-T6 alloy sheets using experimental data obtained from hydroforming tests. The high agreement between predicted and experimentally determined curves demonstrated the potential of AI for modeling the limit deformation behavior of metallic sheets. In [16], a machine learning framework was proposed to estimate FLCs of aluminum alloys from the 5000 and 6000 series using inputs such as chemical composition, mechanical properties, and thermomechanical processing routes. Similarly [17], applied machine learning algorithms to construct FLCs for various steels using tensile properties as input variables. The method showed strong correlation between predicted and experimental values with low average errors, confirming the robustness of AI techniques for characterizing metal formability.

While these studies demonstrate that AI is a promising and efficient alternative for FLC prediction, significantly reducing the need for extensive experimental campaigns, several challenges remain. One of the main limitations is the scarcity of available data—a recurrent issue in metallurgical process modeling. Reduced datasets limit the generalization capability of AI models and may compromise predictive performance. Moreover, recent developments have focused predominantly on ANNs, whereas other machine learning techniques remain underexplored in this context.

In contrast to previous works, which typically train machine learning models directly on small experimental datasets that are often specific to a single alloy or processing route, the present study proposes an integrated framework that combines real experimental data, statistically controlled synthetic data generation, and physically motivated descriptors. The real experimental data play a central role in this work, as they define the physical, statistical, and metallurgical domain of the problem: all multivariate distributions, physical constraints, and statistical validations of the synthetic database are derived from these data. Thus, the synthetic dataset does not replace the real data, but acts as a probabilistic expansion of the experimentally observed space, preserving its physical and statistical correlations. This strategy enables the training of more robust and generalizable machine learning models even when the number of real experiments is limited. In addition, this work advances the state of the art by systematically comparing different machine learning techniques—Random Forest, XGBoost, and Neural Networks—within the same physically consistent database, which remains largely unexplored in the FLC prediction literature.

In this study, different AI techniques are investigated for predicting the Forming Limit Curve of Dual Phase steels using input variables derived from uniaxial tensile tests. To overcome the constraints imposed by the limited availability of experimental data, a physics-guided synthetic database was developed based on metallurgical principles and statistical consistency, ensuring the preservation of the representativeness of real data and preventing biases or distortions that could compromise model integrity. The overarching goal is to broaden the spectrum of learning techniques applied to FLC prediction and to establish a reproducible, scalable, and physically coherent methodology for modeling the formability limits of advanced high-strength steels.

Materials and methods

Figure 1 presents, in a schematic manner, the methodology adopted for the development of Artificial Intelligence (AI) models aimed at predicting the Forming Limit Curve (FLC) of Dual Phase steels. Initially, a robust database was constructed by generating synthetic data derived from real FLCs. This strategy was employed to expand the representativeness and diversity of the available samples. The resulting synthetic dataset was then used in the training, testing, and calibration stages of different predictive models, including Random Forest, XGBoost, and Artificial Neural Networks (ANNs). Finally, the predictive capability of these models was assessed through inference tests conducted exclusively with real experimental data, enabling the evaluation of the effectiveness and generalization capacity of the proposed approaches.

Database construction

The first step in developing an Artificial Intelligence model to predict the Forming Limit Curve (FLC) of Dual Phase steels consists of constructing a comprehensive and

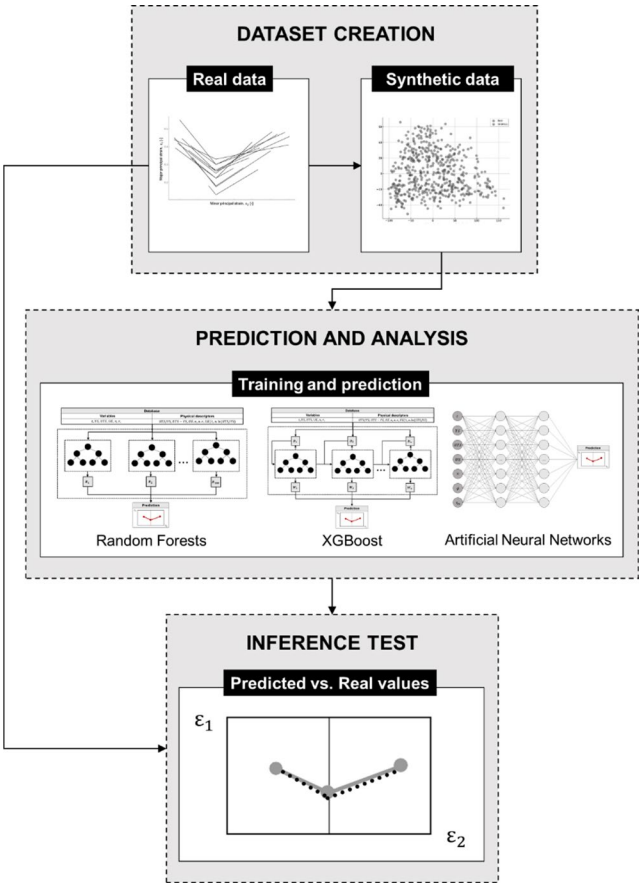

Fig. 1 Methodology employed for predicting the forming limit curves (FLCs) of dual phase steels

technically representative database containing the input parameters required for model training and calibration. For this purpose, experimental data were compiled from studies published in the literature, considering research that investigates the formability of DP580, DP600, DP700, and DP780 steels.

Based on references [18–23], both the published FLCs and the variables known to influence formability were collected. The selected attributes included sheet thickness (t), yield strength (YS), ultimate tensile strength (UTS), uniform elongation (UE), strain hardening exponent (n), and average anisotropy index (r).

Tables 1 and 2 present the set of real experimental data used in this study.These data were selected exclusively from well-established literature sources, published in peer-reviewed scientific journals, and obtained using recognized experimental methodologies. The data exhibit significant scatter, reflecting the physical variability inherent to Dual Phase steels. This variability arises from microstructural heterogeneity (martensite fraction, morphology, and distribution) and from differences in thermomechanical processing routes among manufacturers. This variability does not compromise the validity of the data; rather, it realistically represents the physical domain in which the models must operate. Although the data may contain experimental uncertainties, these do not compromise the objectives of the present work, since the focus of the study is not to fit a deterministic Forming Limit Curve for a specific steel, but rather to evaluate the predictive capability of artificial intelligence models and to establish a robust methodology for FLC prediction based on mechanical properties. In this context, the presence of variability in the data is essential for enabling the models to learn the true statistical behavior of plastic instability, making the predictions more representative and applicable to real industrial conditions.

The Forming Limit Curves were described using three pairs of major (ε_1) and minor (ε_2) principal strains, selected as representative points of the FLC:

$\epsilon_{1(1)}$, $\epsilon_{2(1)}$ located at the left-hand extremity of the curve;

$\epsilon_{1(2)}$; $\epsilon_{2(2)}$ corresponding to the plane strain condition ($\varepsilon_2 = 0$);

Table 1 Real experimental data related to the mechanical properties

Thickness, t [mm]	Yield Strength, YS [MPa]	Ultimate Tensile Strength, UTS [MPa]	Uniform elongation, UE[%]	Strain Hardening Exponent, n [-]	Anisotropy Index, r [-]	Ref.
0,66	379	607	24	0,25	0,99	[18]
0,89	290	662	25	0,25	0,85	[18]
1,42	317	693	25	0,25	0,79	[18]
2,18	376	707	22	0,22	0,76	[18]
1,60	453	714	9	0,13	0,97	[19]
1,20	357	590	24	0,15	1,02	[20]
1,80	345	592	26	0,16	0,99	[20]
1,60	407	777	19	0,12	0,87	[20]
1,50	394	730	22	0,18	0,96	[21]
1,20	399	761	16	0,20	0,82	[21]
1,00	512	795	15	0,16	0,65	[22]
1,50	396	610	24	0,17	0,97	[23]

Table 2 Real experimental data related to the FLCs

Sample	$\epsilon_{1(1)}$	$\epsilon_{1(2)}$	$\epsilon_{1(3)}$	$\epsilon_{2(1)}$	$\epsilon_{2(2)}$	$\epsilon_{2(3)}$	Ref.
1	0,39	0,22	0,43	−0,22	0,00	0,20	[18]
2	0,42	0,25	0,48	−0,21	0,00	0,31	[18]
3	0,38	0,26	0,47	−0,15	0,00	0,34	[18]
4	0,29	0,27	0,46	−0,04	0,00	0,41	[18]
5	0,18	0,13	0,27	−0,04	0,00	0,23	[19]
6	0,44	0,26	0,34	−0,19	0,00	0,18	[20]
7	0,41	0,30	0,39	−0,14	0,00	0,24	[20]
8	0,34	0,22	0,28	−0,14	0,00	0,10	[20]
9	0,55	0,30	0,48	−0,20	0,00	0,38	[21]
10	0,34	0,18	0,38	−0,13	0,00	0,30	[21]
11	0,45	0,18	0,28	−0,23	0,00	0,15	[22]
12	0,44	0,33	0,41	−0,23	0,00	0,40	[23]

$\epsilon_{1(3)}$, $\epsilon_{2(3)}$ representing the biaxial stretching condition at the right-hand extremity of the curve.

This approach makes it possible to synthesize the limit behavior of the material during forming while reducing data dimensionality without losing the essential characteristics of the curve.

Physics-based feature engineering

In order to improve the model's ability to generalize from limited datasets, additional descriptors grounded in physical and metallurgical principles were included in the database. These descriptors do not introduce physical equations into the training process; instead, they provide the machine learning model with physically meaningful input variables that reflect well-known mechanisms of plastic instability in sheet metal forming.

When only directly measured variables are used, the algorithm must autonomously infer nonlinear relationships and complex interactions between mechanical properties and forming limits. By employing physics-guided descriptors as input features, these relationships are explicitly represented in the feature space, reducing the statistical burden on the model, increasing cross-validation stability, and preserving physical coherence in the predictions, without attributing to the model the direct inference of physical causality.

In the specific case of Forming Limit Curve prediction, the different descriptors represent distinct physical effects associated with strain hardening, homogeneous ductility, and geometric stability. Table 3 lists the descriptors employed.

All data were normalized to ensure numerical stability and comparability among variables of different nature and scale. After assembling the complete input vector, composed of the original properties and the physics-guided descriptors, the StandardScaler method was applied, transforming each attribute to a distribution with zero mean and unit standard deviation.

Table 3 Physics-based feature used in the model

Descriptor	Physical Meaning	Motivation for Use
UTS/YS	Ratio between ultimate tensile strength and yield strength	Quantifies strain hardening and the ability to redistribute stresses prior to instability
$UTS - YS$	Difference between ultimate tensile strength and yield strength	Measures the magnitude of strain hardening after yielding
$UE.n$	Product of uniform elongation and strain hardening exponent	Represents the integrated capacity for homogeneous deformation
$n.r$	Interaction between anisotropy and strain hardening	Captures thickness strain stability and resistance to localized necking
UE/t	Ratio between uniform elongation and sheet thickness	Indicator of geometric stability under biaxial deformation
$n.\ln(UTS/YS)$	Ghosh-derived index	Synthesizes combined effects of strain hardening and available post-yield strength

Synthetic data

The limited number of samples in the original experimental dataset constrains the learning capacity of nonlinear regression models. This condition tends to induce overfitting in machine learning models and compromise their ability to generalize. Therefore, a synthetic database was generated without compromising the physical validity or statistical consistency of the original experimental dataset.

The methodology adopted for data generation aimed to satisfy three fundamental requirements:

(i) preservation of the physical–metallurgical domain of the materials under study;

(ii) maintenance of the multivariate relationships between sheet properties and formability; and.
(iii) statistical evidence that the synthetic data are indistinguishable from the real data.

The synthetic database is obtained exclusively through multivariate statistical modeling applied to real experimental data, followed by the application of physicometallurgical plausibility constraints. Thus, the synthetic data represent a statistically consistent expansion of the experimentally observed domain.

Initially, the joint distribution of the input variables

$$x = [t,\ YS,\ UTS,\ UE,\ n,\ r] \tag{1}$$

was modeled using the non-parametric Kernel Density Estimation (KDE) method [24, 25]. This technique approximates the true density $p(x)$ through

$$\widehat{p}(x) = \frac{1}{N\,h^d} \sum\nolimits_{i=1}^{N} K\left(\frac{x - x_i}{h}\right) \tag{2}$$

where K is the Gaussian kernel, h is the bandwidth, and d is the dimensionality. Synthetic samples were drawn according to

$$x_{KDE} \sim \widehat{p}(x) \tag{3}$$

ensuring that sampling occurred only within physically observed regions.

To increase the diversity of combinations in the multivariate space while preserving correlation structure, the KDE samples were projected into the space of Principal Components:

$$z = W^T(x - \mu) \tag{4}$$

and interpolated between randomly selected pairs in this latent representation:

$$z_{new} = \alpha\, z_i + (1 - \alpha)\, z_j + \epsilon \tag{5}$$

where $\alpha \sim U(0,1)$ and ε is low-variance Gaussian noise. Reconstruction into the physical space was obtained via

$$x_{syn} = \mu + W z_{new} \tag{6}$$

configuring a continuous version of the SMOTE concept adapted to the properties of DP steels [26].

This approach enables sampling exclusively within high-probability regions observed in the real data, preventing extrapolation into unrepresented physical domains. Subsequently, to further expand the diversity of feasible combinations without disrupting structural correlations, the data were projected into PCA space and interpolated probabilistically between nearest neighbors—employing a SMOTE-like strategy for continuous multivariate data—combined with controlled smooth noise. This step enhances the generalization potential of the synthetic dataset, particularly in regions with sparse experimental representation.

After generating the input variables, each synthetic sample had its outputs

$$y = \left[\epsilon_{1(1)},\ \epsilon_{1(2)},\ \epsilon_{1(3)},\ \epsilon_{2(1)},\ \epsilon_{2(2)},\ \epsilon_{2(3)}\right] \tag{7}$$

predicted by a Random Forest regression model [27], defined as

$$\widehat{y} = f_{RF}(x_{syn}) \tag{8}$$

where f_{RF} represents an ensemble of decision trees trained exclusively with real data.

However, because this step provides an empirical prediction of mechanical response, additional physical corrections were required to ensure that all synthetic FLCs adhered to problem-specific constraints. The admissible domain for Dual Phase steels was defined by

$$0{,}45 \le \frac{YS}{UTS} \le 0{,}95 \tag{9}$$

To guarantee convexity around the plane strain condition, the following constraints were imposed:

$$\epsilon_{1(2)} < \epsilon_{1(1)},\ \epsilon_{1(2)} < \epsilon_{1(3)} \tag{10}$$

and a minimum separation between branches:

$$\epsilon_{1(j)} - \epsilon_{1(2)} \ge \Delta_{min},\ j \in \{1,3\} \tag{11}$$

Plastic incompressibility was enforced by the approximate constraint:

$$\epsilon_{1(i)} - \epsilon_{2(i)} \ge 0,\ j \in \{1,3\} \tag{12}$$

preventing mechanically infeasible responses.

The quality of the synthetic database was evaluated using the non-parametric Kolmogorov–Smirnov (KS) test applied individually to each variable [28]:

$$D = sup_x \left|\widehat{F}_{syn}(x) - \widehat{F}_{real}(x)\right| \tag{13}$$

The associated p-value was used to test the null hypothesis

$$H_0 : \widehat{F}_{syn}(x) = \widehat{F}_{real}(x) \tag{14}$$

To ensure statistical rigor, a Bonferroni correction [29] was applied to account for multiple testing. Considering 12 variables, a global significance threshold of

$$\alpha^* = \frac{0{,}05}{12} = 0{,}0042 \tag{15}$$

was required, meaning that the synthetic set was accepted only when all variables satisfied

$$p_{KS} \geq \alpha^* \tag{16}$$

indicating strong statistical indistinguishability between real and synthetic distributions.

Correlation matrices and PCA projections were also analyzed, confirming visual overlap and preservation of structural dependencies between material properties and mechanical response. The combination of these criteria resulted in a synthetic dataset that is statistically indistinguishable from the original and fully consistent with the physical relationships inherent to the system studied.

To prevent information recycling between synthetic and experimental data, a strict separation was enforced between data generation, model training, and performance evaluation. The real experimental data were used only to calibrate and statistically validate the synthetic data generator, as well as for the final inference tests. All training, hyperparameter tuning, and cross-validation of the artificial intelligence models were performed exclusively on the synthetic dataset. Performance metrics (MAE, MSE, and R^2) were computed only from predictions on real experimental data that were not used during training, ensuring that the reported results reflect the models' generalization capability to physical data. In addition, the synthetic data generation is stochastic and based on statistically validated multivariate distributions, which prevents the simple replication or direct interpolation of individual experimental points.

This methodology ensures that the synthetic data not only expand the number of observations available to the predictive model, but also preserve, in a statistically consistent manner, the physical and metallurgical relationships observed in the experimental data within a physically admissible domain. In this way, the synthetic data provide a reliable basis for training artificial intelligence models and for subsequent scientific analyses, without attributing to them the ability to independently infer physical causality.

Artificial intelligence model

The selection of the Artificial Intelligence technique must account for the specific characteristics of the dataset. Forming Limit Curve prediction constitutes a multi-output regression problem characterized by high nonlinearity and strong coupling between variables. The available dataset is small, heterogeneous, and affected by experimental noise. Based on these constraints, three machine learning techniques were investigated: Random Forest, XGBoost, and Artificial Neural Networks.

Random Forest (RF) is a machine learning method based on an ensemble of multiple decision trees. Each tree is trained using a random subset of samples and predictors, and the final output is obtained through voting (for classification) or averaging (for regression). This approach reduces the risk of overfitting, which is common in individual trees, thereby yielding a more robust and accurate model [30]. RF tends to perform well even on small and heterogeneous datasets because its random sampling (bagging) strategy increases diversity among trees and reduces overfitting risk [31].

XGBoost, in turn, uses an ensemble of decision trees trained sequentially, where each new tree is constructed to correct the errors of the previous ones. This gradient-boosting mechanism enables the model to learn subtle and complex relationships between the input variables and the multiple outputs of the problem [32]. Unlike Random Forest—which aggregates independent trees—XGBoost progressively adjusts the model to minimize a global loss function, achieving high predictive accuracy even in systems with non-trivial interactions, such as the one investigated here. Moreover, XGBoost incorporates internal regularization mechanisms that prevent overfitting and enable good generalization on small and heterogeneous datasets. Its computational efficiency and the ability to automatically weight variable importance make it particularly powerful for modeling complex metallurgical phenomena with experimental noise and multiple physical dependencies [33].

The potential of Artificial Neural Networks (ANNs) for predicting Forming Limit Curves lies in their ability to handle problems involving highly nonlinear relationships and strong coupling among multiple variables. Inspired by the functioning of the human brain, ANNs consist of layers of interconnected neurons that transform input variables into outputs through adjustable mathematical functions (synaptic weights). During training, the network learns to adjust these weights to minimize the error between predictions and experimental values, enabling it to capture complex and subtle patterns even in metallurgical systems with nonlinear behavior [34].

In scenarios with small datasets and experimental noise—common in forming tests—ANNs require complementary techniques such as regularization, cross-validation, and synthetic data augmentation to avoid overfitting. When properly configured, however, they offer high generalization capability and can predict multiple outputs simultaneously, modeling in an integrated manner the plastic behavior and the influence of material parameters [35]. Thus, ANNs stand out as a flexible and powerful approach for representing the complex behavior of Forming Limit Curves.

The architecture of each model was defined through a hyperparameter optimization procedure based on an intelligent search strategy, using the minimization of the Mean Absolute Error (MAE) as the objective function. To prevent bias and overfitting, repeated cross-validation was employed, increasing the statistical robustness of the estimates—particularly important given the limited number of real samples. At each iteration of the search, hyperparameters were dynamically adjusted to ensure that the model achieved maximum performance without loss of generalization. Early stopping was implemented as an additional safeguard, interrupting training when no further improvements in validation performance were observed.

Data preprocessing

The raw dataset was subjected to a preprocessing stage to transform it into a structured and consistent format suitable for training machine learning models. The input vector was constructed using a domain-informed feature engineering approach, combining metallurgical and statistical knowledge. Two main groups of independent variables were defined:

(i) basic mechanical properties of the material: t, YS, UTS, UE, n, r; and.
(ii) physics-guided descriptors, obtained from combinations or functional relationships among the original variables: UTS/YS, $UTS - YS$, $UE.n$, $n.r$, UE/t, $n.\ln(UTS/YS)$

The concatenation of these two groups resulted in the final feature vector (feature_cols), integrating both raw properties and higher-order descriptors that are potentially more correlated with the formability phenomenon under investigation.

The problem was formulated as a multi-output regression, in which the target variables (matrix y) correspond to the six characteristic points of the Forming Limit Curve (FLC)—from $\epsilon_{1(1)}$ to $\epsilon_{2(3)}$—requiring the models to simultaneously predict all limit strain values.

The dataset was split into training (80%) and testing (20%) subsets using the train_test_split function from the Scikit-learn library. Finally, Z-score normalization was applied using the StandardScaler, ensuring that all attributes were transformed to have zero mean and unit standard deviation—an essential condition for the stability and efficiency of the supervised learning algorithms employed.

Evaluation of predictive performance

A quantitative and unbiased evaluation of the predictive performance of the trained models was carried out using the test set (X_test_scaled, y_test), which was kept completely isolated throughout the parameter-tuning and training stages. Each model was used to generate independent predictions for the test data, allowing a direct comparative analysis under identical inference conditions.

Predictive performance was quantified using three standard regression metrics, widely adopted in continuous modeling problems:

(i) Mean Absolute Error (MAE), which measures the average absolute difference between predicted and observed values, expressed in the same units as the target variables and exhibiting robustness to outliers;
(ii) Mean Squared Error (MSE), which computes the average of squared errors and penalizes larger discrepancies more strongly; and.
(iii) Coefficient of Determination (R^2), an indicator of the proportion of variance explained by the input variables.

Inference tests

The inference tests constituted the final validation stage of the models and were performed using data not employed during training. In this phase, only real experimental data were used, enabling an assessment of the models' generalization capability and predictive performance under practical conditions. This stage is essential to verify whether the models—previously calibrated using the synthetic dataset—are capable of accurately reproducing the behavior observed in real measurements, ensuring their applicability and reliability in predicting the Forming Limit Curves of Dual Phase steels.

Results and discussion

Analysis of the database

Figure 2 presents the correlation coefficients between the properties of the evaluated Dual Phase steels and the characteristic points of the Forming Limit Curve (FLC). Uniform elongation exhibits the strongest positive correlations with

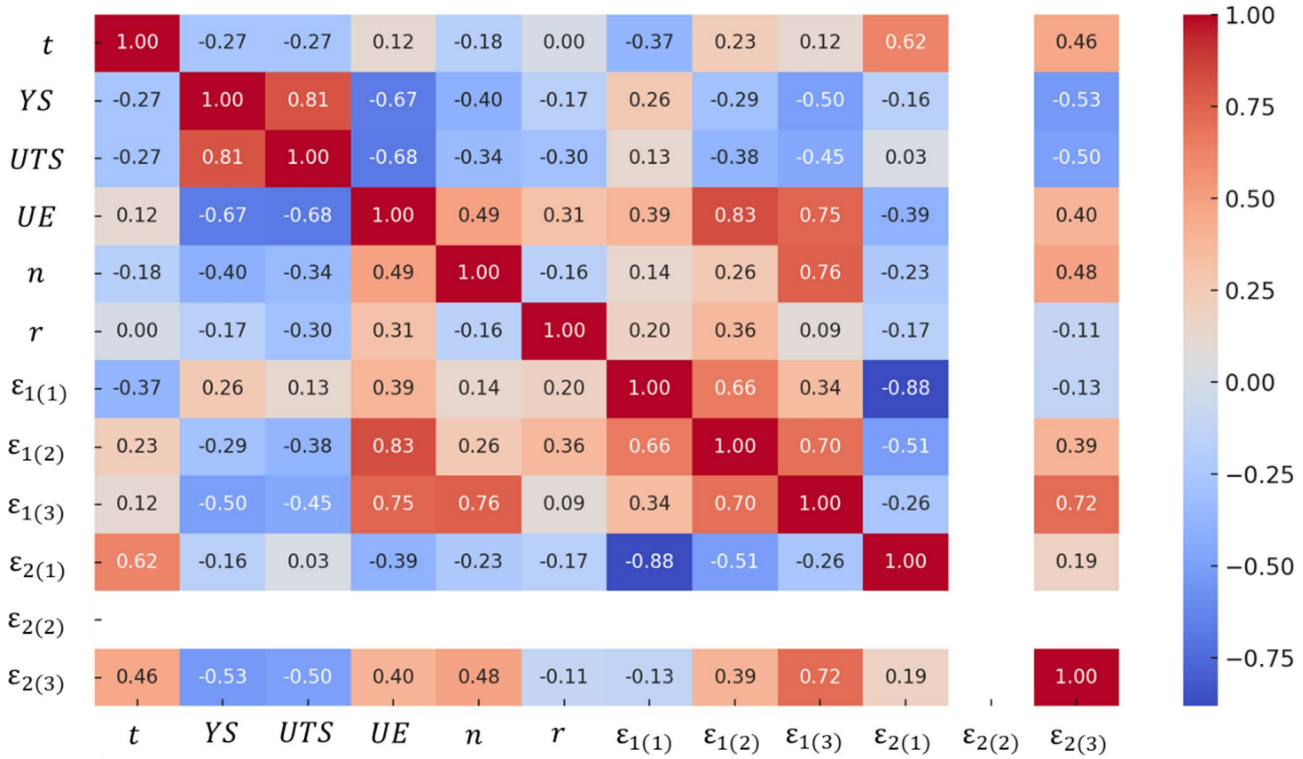

Fig. 2 Correlation coefficients between the properties of the dual phase steels and the characteristic points of the forming limit curve

the ε_1 points, particularly $\epsilon_{1(2)}$ and $\epsilon_{1(3)}$, indicating that global ductility acts as the primary stabilizing factor against localized necking under plane-strain and biaxial stretching conditions.

The strain hardening exponent n also shows a marked positive correlation with $\epsilon_{1(3)}$ reflecting the role of work hardening in promoting stress redistribution and delaying the onset of localized instability, in agreement with classical predictions of the Marciniak–Kuczinski instability model [36, 37].

In contrast, mechanical strength exerts an opposite effect. Negative correlations—although of moderate magnitude—were observed between yield strength, tensile strength, and $\epsilon_{2(1)}$, demonstrating that increases in strength tend to reduce the material's formability. This behavior is consistent with the well-established relationship between higher flow stresses and diminished strain accommodation capacity in sheet metals.

The sheet thickness, in turn, exhibited a significant positive correlation with the ε_1 points, confirming the expected increase in formability with increasing material thickness [38]. The anisotropy coefficient r showed moderate positive correlations with $\epsilon_{1(1)}$ and $\epsilon_{2(1)}$ As r increases, the strain paths tend to shift leftward, and higher values of r_m also allow larger ε_1 strains to be achieved in the negative minor-strain region ($\varepsilon_2 < 0$) [39].

The set of relationships observed reveals that the formability of DP steels depends predominantly on the combination of homogeneous ductility and strain hardening capacity, whereas higher strength tends to reduce the forming limit, particularly under more critical strain paths. In addition, thickness plays a complementary role in controlling instability. The physical coherence of the correlations obtained reinforces the adequacy of the selected variables as input descriptors for developing machine-learning-based predictive models of the FLC.

Given the use of synthetic data, assessing the statistical adherence to real data becomes essential. Figure 3 shows the histograms of the input variables in the database. The distributions of the input variables were well preserved—and even expanded—in the synthetic dataset. This is essential for AI models, as it ensures that the model does not learn only the patterns present in the real samples but also gains sufficient variability to generalize effectively to unseen data.

The synthetic thickness distribution closely follows the real distribution, with the inclusion of a few intermediate combinations that do not lead to undue extrapolation. This added variability benefits the training of machine-learning models while remaining within the typical thickness range for the material.

The YS and UTS values exhibit a more dispersed distribution in the synthetic dataset. This broader spread

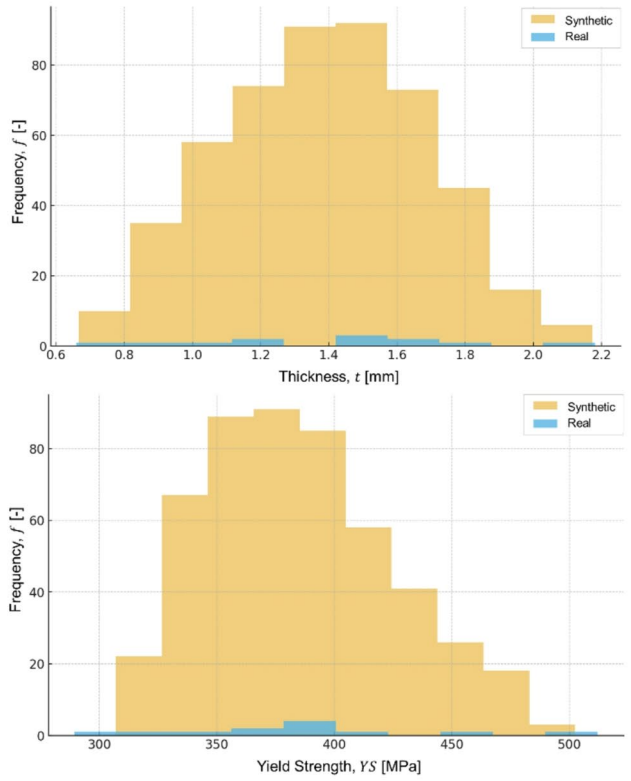

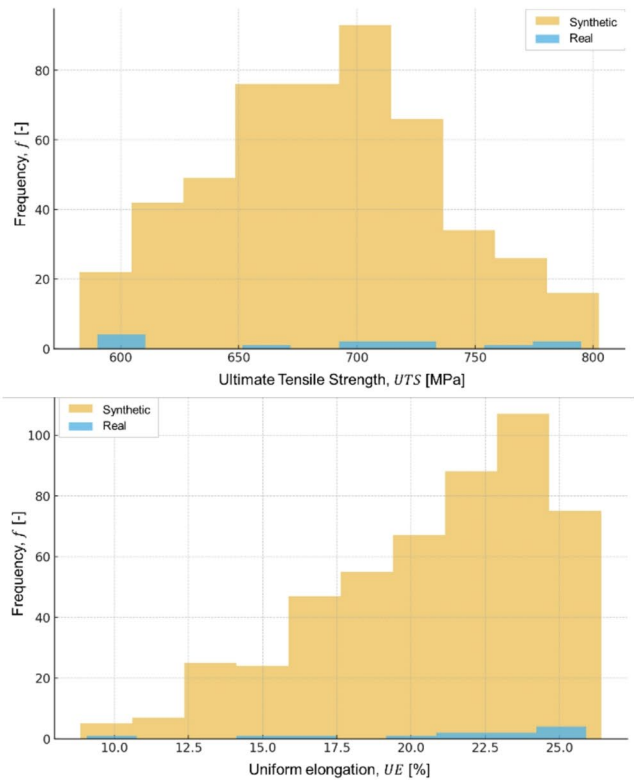

Fig. 3 Histograms of the input variables in the database

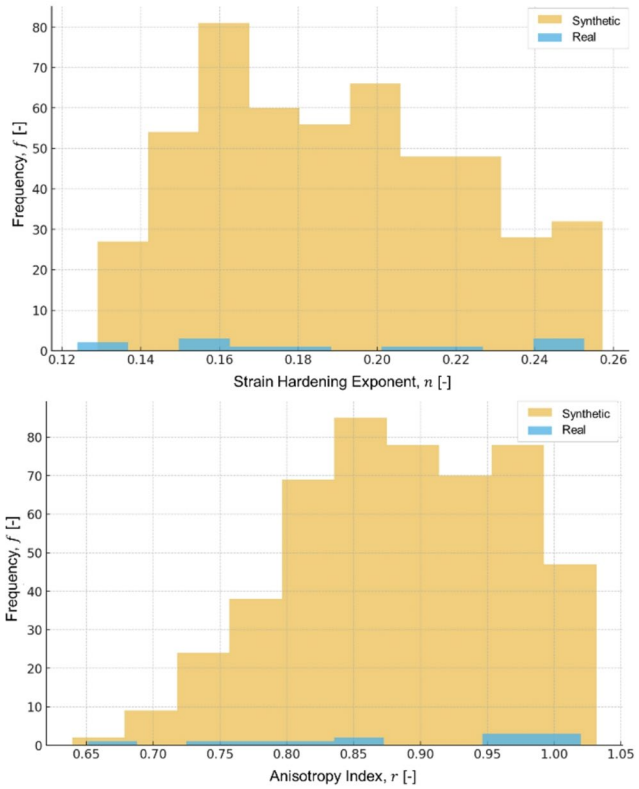

Fig. 3 (continued)

improves generalization by allowing the AI model to better capture the nonlinear relationships between yield strength and tensile strength, a common feature in high-strength metallic alloys. For AI applications, such dispersion helps mitigate overfitting—an issue frequently encountered in small experimental datasets.

The synthetic dataset does not extrapolate beyond the physical domain of the experimental data, but rather provides a statistical densification of the already observed space. For all variables, the synthetic values remain confined within the envelope defined by the real data and by the physically admissible ranges for Dual Phase steels in the DP580–DP780 classes. The apparent increase in dispersion in the synthetic dataset results from the continuous filling of intermediate regions between experimental points, rather than from the generation of combinations outside the experimental domain. This densification of the sample space allows the machine learning models to more fully explore the nonlinear correlations between mechanical properties and formability, while simultaneously preserving the physical limits of the problem.

Figure 4 displays all FLCs from both the synthetic and real databases. The distribution of the synthetic curves follows the behavior of the real curves, with a controlled expansion of variability to ensure that the machine-learning

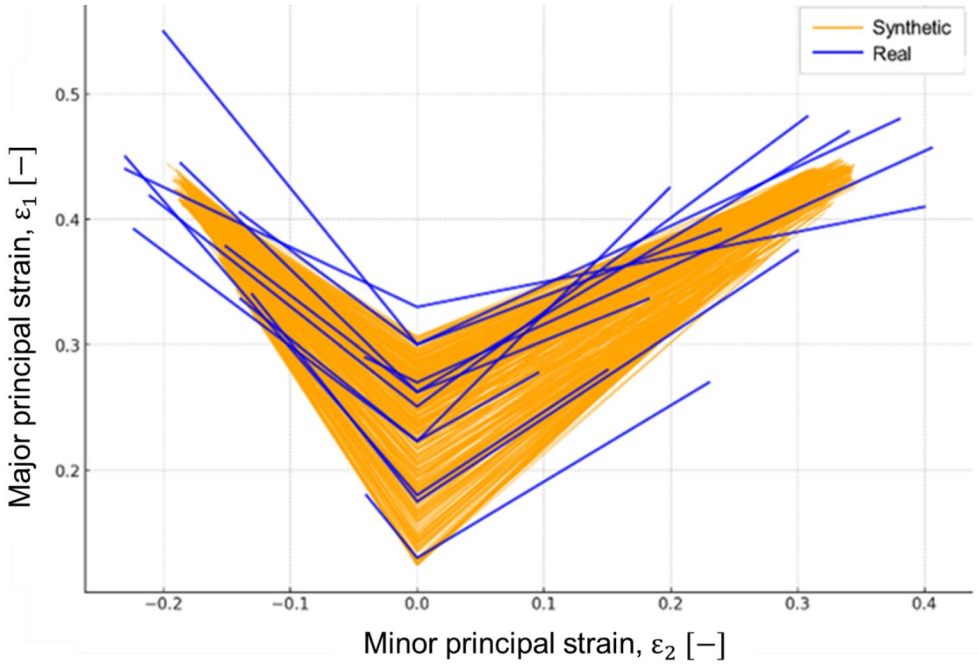

Fig. 4 Synthetic and real Forming Limit Curves [18–23]

model is exposed to sufficient diversity to generalize effectively. The dispersion remains confined to physically plausible regions and does not extrapolate into unrealistic forming behaviors.

Table 4 presents the results of the Kolmogorov–Smirnov (KS) test for each variable in the synthetic database. All variables, both inputs and outputs, exhibit p-values higher than 0.0042 after the Bonferroni correction. This indicates that there is no statistical evidence to reject the null hypothesis; in other words, the real and synthetic distributions are considered indistinguishable at the 5% significance level when accounting for multiple testing.

Table 4 Kolmogorov–Smirnov (KS) test results for each variable in the synthetic database

Variable	KS-stat	*p*-valor	Bonferroni (*p**12)
Thickness, t [mm]	0.1407	0.9496	1.0000
Yield Strength, YS [MPa]	0.1547	0.9018	1.0000
Ultimate Tensile Strength, UTS [MPa]	0.2673	0.3138	1.0000
Uniform elongation, UE[%]	0.2660	0.3196	1.0000
Strain Hardening Exponent, n [-]	0.1980	0.6786	1.0000
Anisotropy Index, r [-]	0.2700	0.3031	1.0000
$\epsilon_{1(1)}$	0.3313	0.1201	1.0000
$\epsilon_{1(2)}$	0.2220	0.5387	1.0000
$\epsilon_{1(3)}$	0.3333	0.1161	1.0000
$\epsilon_{2(1)}$	0.4260	0.0192	0.2304
$\epsilon_{2(2)}$	0.0000	1.0000	1.0000
$\epsilon_{2(3)}$	0.3113	0.1659	1.0000

The variable $\epsilon_{2(1)}$ exhibits a p-value of 0.0192 and a Bonferroni-adjusted value of 0.2304. Although it is the only p-value below 0.05, it remains well above the critical threshold of 0.0042; therefore, there is no evidence to reject distributional similarity. This variable showed greater sensitivity to the initial physical projections. Consequently, a complementary probabilistic equalization step was performed using conditional quantile mapping, incorporating the combined effects of UE, n, and r on the statistical positioning of this specific FLC point. This strategy softened the probability accumulation near the numerical boundaries imposed by the physical repairs while preserving the physical linkage to global ductility, avoiding rigid caps that would artificially reduce the original variance. As a result, an appropriate balance between physical consistency and statistical variability was achieved.

The analysis of the Empirical Cumulative Distribution Function (ECDF) plots (Fig. 5) for the synthetic database variables enables a detailed assessment of the quality of the generated data. The ECDF curves reveal that the cumulative distributions of the synthetic data closely follow those of the real data. This indicates that the synthetic database was generated in a manner that preserves the fundamental statistical properties of the variables observed in the real dataset.

The real and synthetic curves exhibit extensive overlap, demonstrating that the synthetic samples are distributed very similarly to the real ones, without significant distortions or extrapolation into regions not supported by the

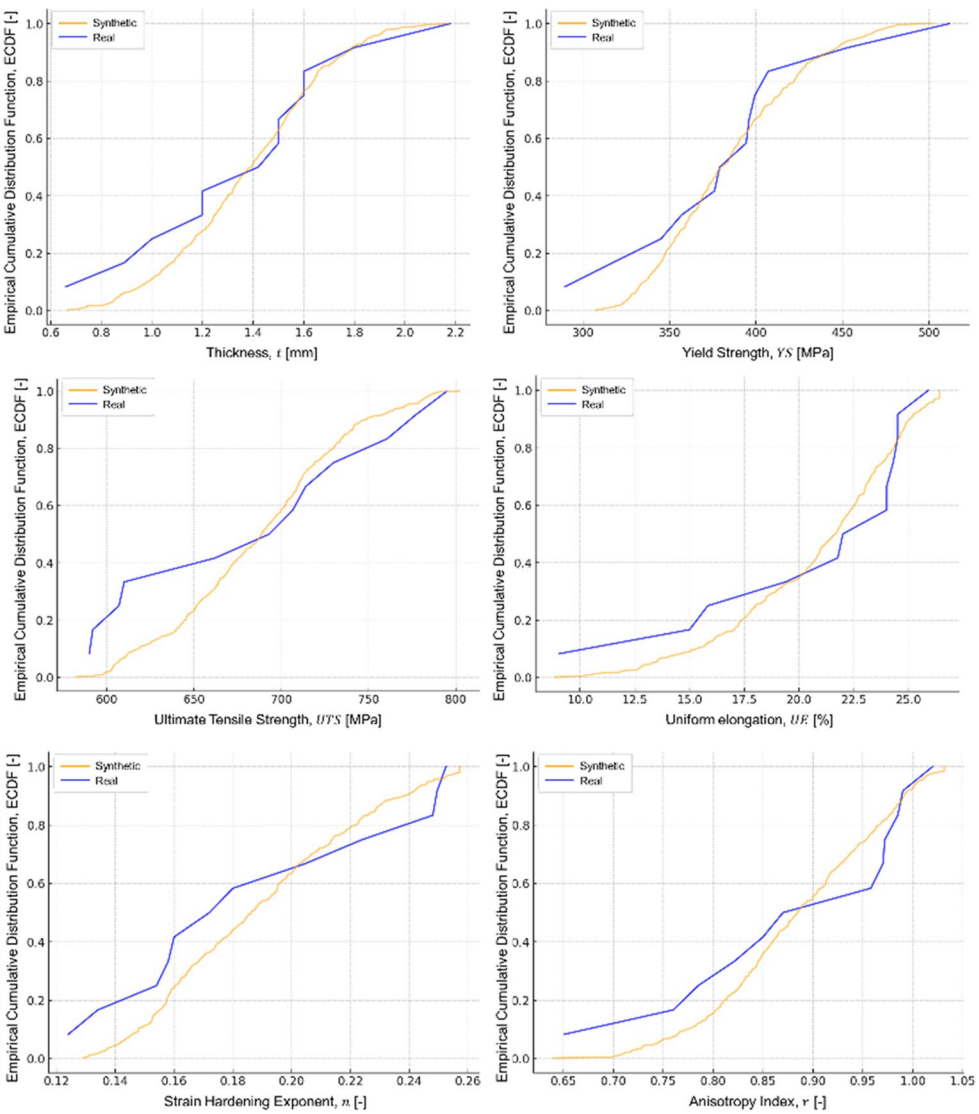

Fig. 5 Empirical Cumulative Distribution Function for the input and output variables

original data. This behavior is particularly important, as it shows that the synthetic dataset successfully captures the natural variability present in the real measurements without introducing bias or modeling artifacts.

The Principal Component Analysis (PCA) plot (Fig. 6) provides a view of the multivariate distribution of the data in the reduced space of the first two principal components. This plot is intended to assess the preservation of multivariate structure and the degree of similarity between the real and synthetic data. The dispersion of points shows that the synthetic samples do not deviate significantly from the real ones, suggesting that the synthetic data generation procedure was successful in maintaining the global variability observed in the real variables. This is crucial to ensure that the synthetic database provides a robust foundation for training AI models without introducing bias or distortions into the dataset.

Random forest (RF) model

The Random Forest (RF) model was developed with the objective of serving as a reference (baseline) approach for the simultaneous prediction of the six characteristic points of the Forming Limit Curve (FLC). Because the random forest algorithm does not natively support multi-output prediction, an encapsulation strategy was adopted to enable multi-output regression. In this configuration, an independent model was trained for each target variable, resulting in six distinct forests, all based on the same underlying architecture but individually adjusted according to their respective output vectors. This approach allows the method to treat each characteristic FLC point autonomously, avoiding cross-coupling between responses and preserving both the stability and computational simplicity of the model.

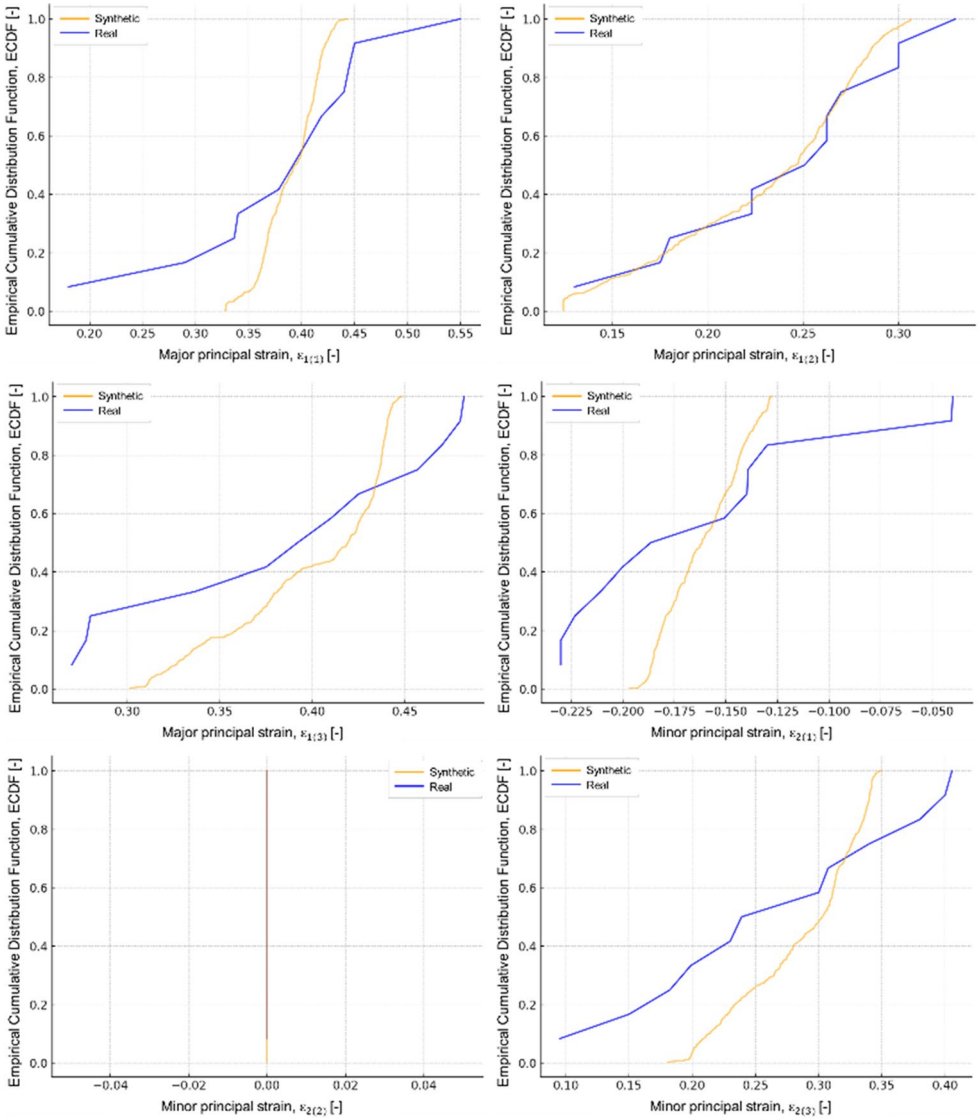

Fig. 5 (continued)

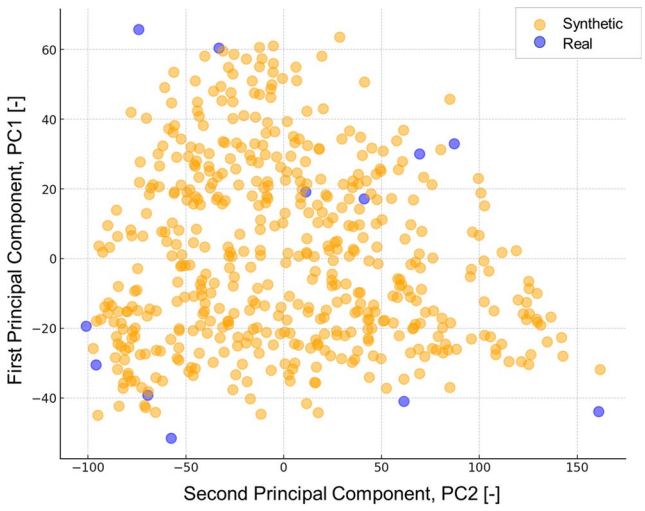

Fig. 6 Principal Component Analysis

Figure 7 presents a conceptual schematic of the operating principle of the Random Forest model applied to the prediction of the Forming Limit Curve (FLC). The diagram illustrates the flow of information from the input database to the generation of the final predictions of the limit strains (ε_1 and ε_2).

The methodology consists of forming an ensemble of independent decision trees, denoted $R_1,\ R_2, \ldots, R_{100}$ each trained with different randomly selected subsets of data and variables. This variability introduced into each tree is essential for increasing the diversity of the individual models, reducing the correlation among them and, consequently, lowering the risk of overfitting.

During inference, each tree independently predicts the FLC values. The individual predictions are then aggregated through arithmetic averaging, resulting in a more stable and

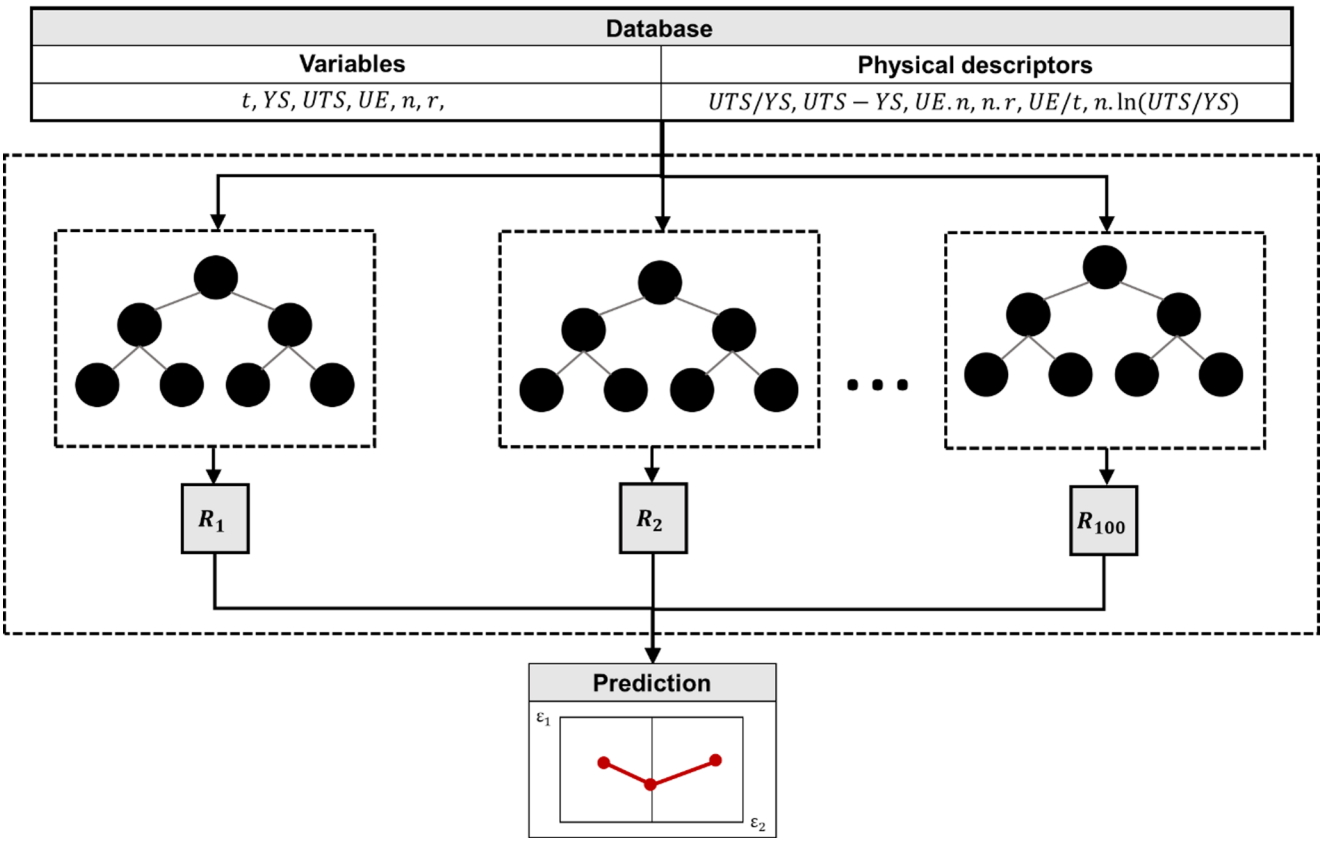

Fig. 7 Operating principle of the XGBoost model applied to the prediction of the forming limit curve (FLC)

accurate final response. This combination strategy, characteristic of ensemble learning, allows the model to robustly capture nonlinear and complex relationships between the material properties and its limit formability behavior.

Each forest was composed of 100 decision trees, whose predictions were combined by arithmetic mean. This configuration ensures a high capacity to model nonlinearities while simultaneously reducing the variance of the estimates. Procedures were adopted to ensure reproducibility of the results and to exploit parallel processing, optimizing training time even in a multi-output scenario.

XGBoost model

The final architecture of the XGBoost model developed for predicting the Forming Limit Curve (FLC) adopted a multi-target configuration, which demonstrated superior performance after systematic hyperparameter optimization. The model is composed of six independent regressors, each responsible for estimating one characteristic point of the FLC, trained simultaneously.

Figure 8 schematically illustrates the operating principle of the XGBoost model applied to FLC prediction. The method consists of an ensemble of weak learners (decision trees) trained iteratively, where each tree is fitted to the residuals of the accumulated model and then combined through a weighted sum.

From the input database, the algorithm sequentially constructs different decision-tree models, represented by the intermediate blocks associated with $D_1,\ D_2, \ldots,\ D_n$. Each set D_i symbolizes the state of the data at a given boosting iteration — that is, the residual information (errors) that guides the training of the next tree to correct the deficiencies of the previous one. The weights assigned to each tree within the ensemble, $W_1,\ W_2,\ \ldots,\ W_n$ are updated during training according to the contribution of each estimator to the reduction of the global loss.

The final multi-target architecture of the XGBoost model for Forming Limit Curve prediction was configured with a maximum tree depth of 3, which helped limit the complexity of the internal partitions and consequently reduced the risk of overfitting in an inherently small dataset. A total of 3000 sequential decision trees were used as estimators, favoring incremental knowledge construction and allowing subtle nonlinear patterns between the steel properties and the characteristic FLC points to be progressively captured. The learning rate was set to a moderately low value (0.03), ensuring that each new estimator performed fine-grained corrections on the residuals of the previous model, with significant impact on training stability.

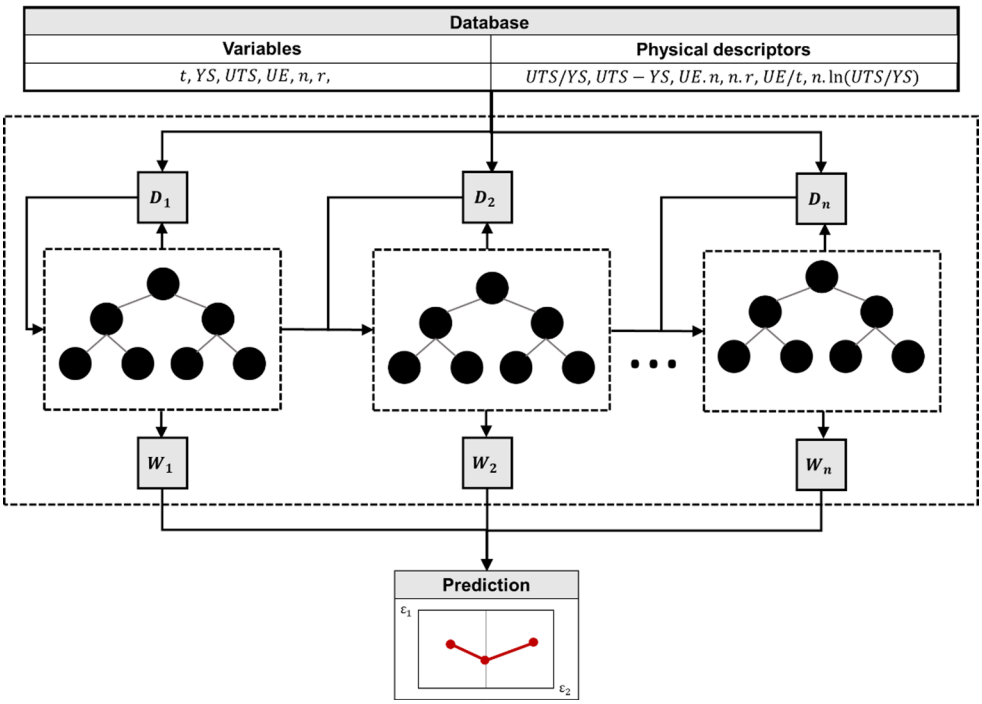

Fig. 8 Operating principle of the artificial neural network (ANN) model used for predicting the forming limit curve (FLC)

Regarding regularization, the $L2\,(\lambda = 10)$ and $L1\,(\alpha = 0.2)$ penalties acted jointly to restrict excessively large leaf weights, controlling model complexity and preventing noisy or atypical values in the synthetic dataset from causing artificial extrapolations. Additionally, stochastic subsampling strategies were employed, using 92% of the records for each tree and 79% of the available features per split. These measures substantially increase structural diversity among the trees and reinforce the statistical robustness of the boosting ensemble.

Artificial neural network model

Figure 9 presents the conceptual schematic of the Artificial Neural Network (ANN) architecture employed for predicting the Forming Limit Curve (FLC). The diagram illustrates

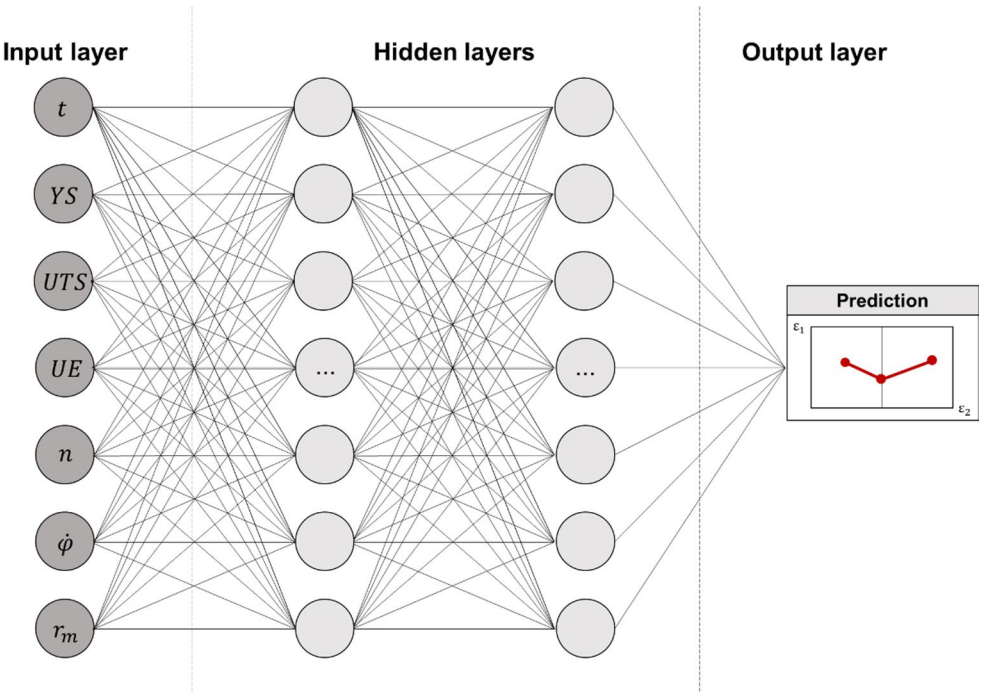

Fig. 9 Operating principle of the Artificial Neural Network (ANN) model used for predicting the Forming Limit Curve (FLC)

the typical structure of a multilayer feedforward network (Multilayer Perceptron – MLP), consisting of an input layer, multiple hidden layers, and a multivariate output layer.

In the input layer, the model receives the attributes of the dataset (material properties and physics-guided descriptors). The hidden layers constitute the core of the learning process. Each neuron in these layers performs a nonlinear transformation of the inputs through its activation function, enabling the network to model the complex and strongly nonlinear behaviors characteristic of plastic deformation processes. The number of layers and neurons was tuned to balance learning capacity and generalization.

The output layer contains six linear neurons, corresponding to the six characteristic points of the FLC, such that the network performs a multi-output regression, simultaneously predicting all limit strain values.

The final ANN architecture consists of fully connected layers, using the Rectified Linear Unit (ReLU) activation function in the hidden layers and linear activation in the output layer, which is appropriate for continuous target variables. The model comprises three hidden layers with 256, 128, and 64 neurons, designed to capture highly nonlinear patterns and complex interactions among the input variables.

The model was optimized using the Adam algorithm and trained with the Mean Absolute Error (MAE) loss function, selected for its robustness to outliers and its direct physical interpretability. Training was limited to 200 epochs, with an Early Stopping strategy implemented to prevent overfitting. The validation metric (mean absolute error on the validation set) was monitored at every epoch, and training was automatically halted if no improvement occurred for 20 consecutive iterations. In such cases, the weights corresponding to the best validation performance were restored. This regularization strategy provided enhanced stability and generalization capability in the presence of variability and experimental noise within the dataset.

Predictive performance of the AI models

Figure 10 presents the distribution of absolute errors for the three evaluated models at the main characteristic points of the Forming Limit Curve (FLC). Overall, all models exhibit low error magnitudes, indicating good generalization capability in predicting the FLC. However, important differences arise when examining specific regions of the curve and the behavior of each model.

At the points associated with regions $\epsilon_{1(2)}$ and $\epsilon_{2(3)}$, a larger dispersion of errors and a higher occurrence of outliers are observed. This reflects the intrinsic complexity of these transitional zones of the material's limit behavior, where small experimental uncertainties lead to greater variability in the positioning of the curve points. In contrast, the $\epsilon_{1(1)}$ points exhibit substantially lower errors and more compact distributions, indicating greater physical and predictive stability in these regions.

Figure 11 provides a direct comparison of the Mean Squared Error (MSE) among the three models. The extremely low MSE values — on the order of 10^{-4} for all models—reinforce that each method adequately captures the relationships between the input variables and the characteristic points of the Forming Limit Curve.

The comparative analysis reveals marked performance differences. The Random Forest model displays the most consistent behavior among the evaluated techniques, with MAE = 0.0052, lower medians, and reduced interquartile ranges across nearly all points analyzed. It also presents the lowest MSE (0.00011), underscoring its favorable combination of low variance and robustness to experimental noise. This characteristic is particularly relevant in metal forming studies, where small fluctuations in testing conditions frequently introduce systematic uncertainties.

The XGBoost model exhibits intermediate performance, with an MAE of 0.0062 and medians close to those of the

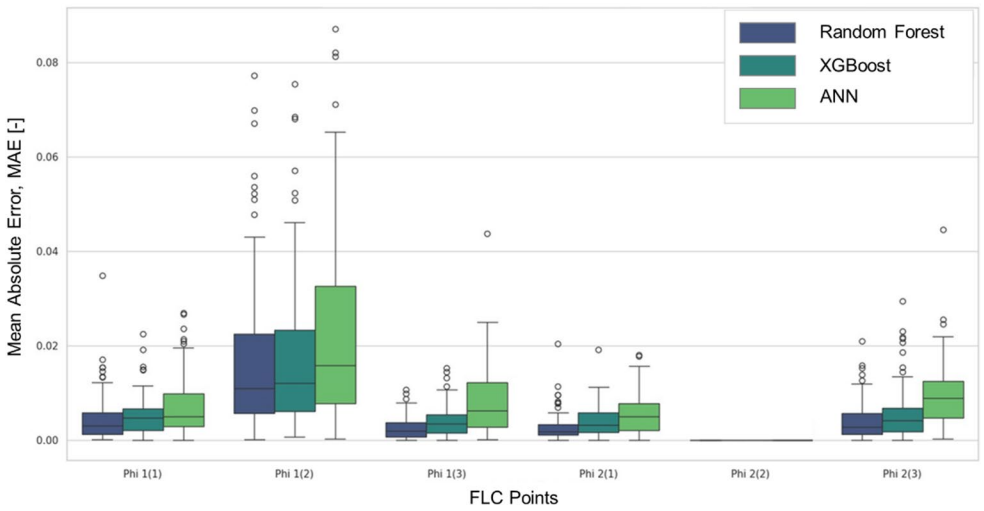

Fig. 10 Distribution of absolute errors for the three evaluated models

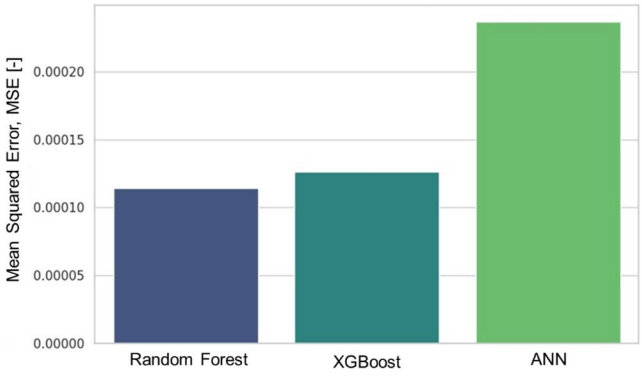

Fig. 11 Mean squared error values for the three evaluated models

Random Forest. However, it shows a greater tendency to produce extreme values in critical regions such as $\epsilon_{1(2)}$. This behavior is consistent with the iterative nature of boosting, which emphasizes residual errors and therefore becomes more sensitive to local fluctuations in the data. Its MSE (0.00012) is slightly higher than that of the Random Forest, although still very close, indicating that the model is capable of capturing complex relationships within the dataset, but with somewhat lower statistical stability.

The Neural Network, in turn, although producing medians comparable to those of the tree-based approaches, exhibits an MAE of 0.0092 and a higher number of outliers, particularly at the points $\epsilon_{1(2)}$, $\epsilon_{2(1)}$, and $\epsilon_{2(3)}$.This greater dispersion suggests a tendency toward overfitting, even after hyperparameter optimization, likely due to the limited amount of data available to train a relatively deep architecture. Consequently, the network's MSE (0.00024) is approximately twice that of the ensemble models, indicating greater difficulty in generalizing from the experimental dataset. Such behavior is typical when the complexity of the network exceeds the amount of information available, leading the model to memorize specific patterns from the training set at the expense of global predictive capability.

The R^2 values presented in Fig. 12 reveal clear differences in the generalization capability of the evaluated models. The

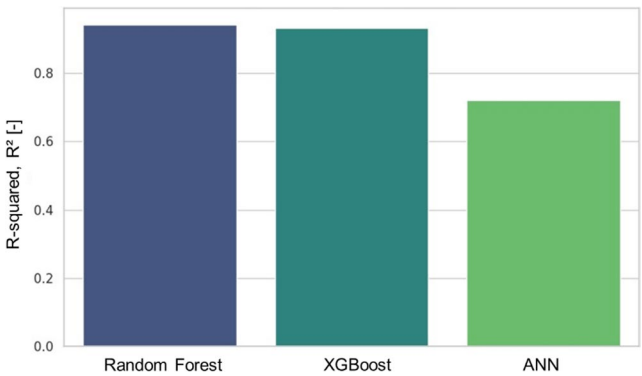

Fig. 12 Coefficient of determination values for the three evaluated models

Random Forest exhibits the best overall performance, with $R^2 = 0.943$, indicating that the model explains more than 94% of the total variability associated with the characteristic points of the Forming Limit Curve. This result corroborates the robustness observed in the other metrics—particularly the low absolute errors and the smallest MSE—reinforcing that the Random Forest efficiently captures both the nonlinearities and the interactions among the input variables.

The XGBoost model achieves an $R^2 = 0.9336$, very close to the Random Forest, demonstrating similarly high predictive performance. The slight difference between the two models is consistent with the trends observed in the error distributions. XGBoost shows slightly greater sensitivity to experimental noise, which is reflected in the small reduction in explanatory power. Nevertheless, it remains a highly effective model, capable of accurately reproducing the overall geometry of the FLC.

The neural network, in contrast, attains an $R^2 = 0.717$, substantially lower than the ensemble-based models. This value indicates that approximately 28% of the total variability remains unexplained, which aligns with its higher MSE and the greater dispersion observed in the boxplots. This reduced performance reflects the typical limitations encountered when the dataset size is relatively small for a deep architecture, favoring overfitting and reducing generalization capability.

The inference tests further support the conclusions drawn from the previously analyzed metrics. Figure 13 shows the absolute error distributions for the three models, revealing distinct statistical patterns. In all cases, the distribution exhibits positive skewness, with a strong concentration of predictions near zero error and a long tail associated with more discrepant estimates. This behavior is characteristic of regression models in which most observations are well represented.

For the Random Forest, the error distribution is the most concentrated among all evaluated models. A clearly defined peak is observed at values below 0.005, followed by a rapid decline in frequency as the error increases. The tail is less pronounced and virtually nonexistent above 0.03. Such behavior indicates that the Random Forest not only provides low average error but also displays high statistical consistency, with limited variability and few extreme deviations. The estimated density reinforces the presence of a single well-defined mode, suggesting strong stability across the entire FLC domain.

The XGBoost model exhibits a similar distribution, but with slightly greater dispersion and a more frequent occurrence of errors in the range of 0.01 to 0.03. The estimated density shows a smoother profile, with a mode also located at very low values, yet accompanied by a longer tail compared to the Random Forest. This behavior confirms that

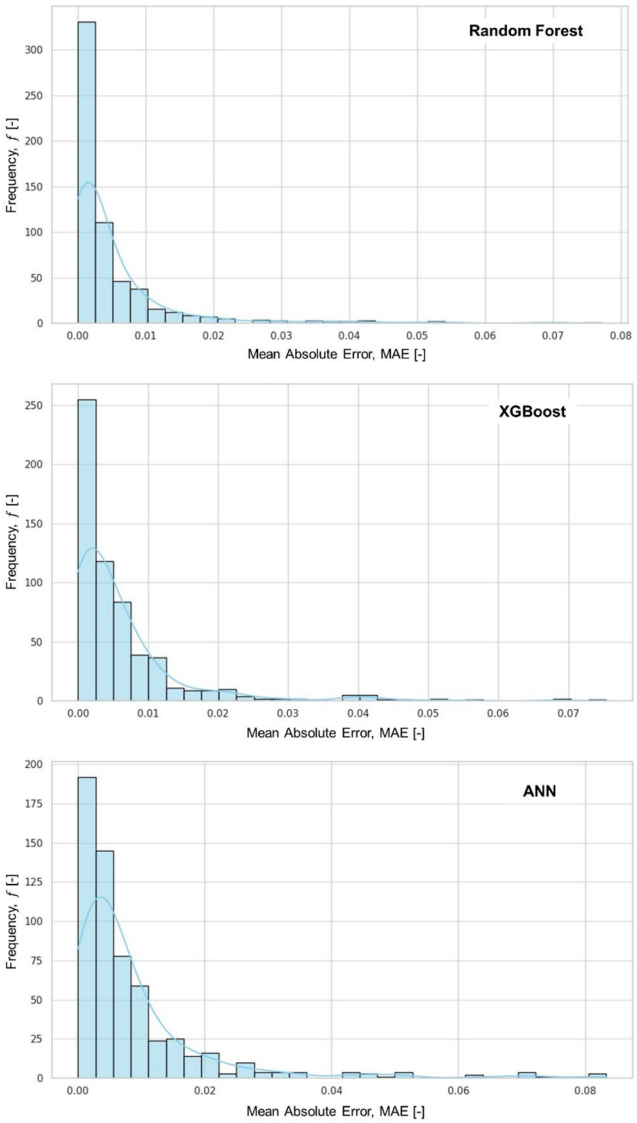

Fig. 13 Absolute error distributions of the models in the inference tests

XGBoost maintains strong predictive capability but is more sensitive to local irregularities and noise within the data.

The Neural Network presents the most dispersed error distribution among the evaluated models. Although it also exhibits a mode near zero, the frequency of errors above 0.01 is considerably higher, and the tail extends to values exceeding 0.08. The density curve is noticeably flatter, indicating reduced concentration of errors around the mean and increased variability. This pattern is typical of models affected by overfitting or constrained by insufficient data volume to adequately learn the complexity of the problem.

From a statistical inference perspective, the observed differences among the distributions indicate that the Random Forest is the most robust model—not only because it delivers the lowest mean error, but also because it demonstrates lower variance, reduced skewness, and lighter tails. XGBoost closely follows this behavior, though with a slightly higher propensity for moderate errors. The Neural Network, by contrast, displays a distribution with greater variability and a heavier tail, reflecting inferior performance.

Figure 14 presents examples of FLCs from the inference test set. The examples presented show curves with significantly different behaviors, yet all models were able to accurately reproduce the characteristic geometry of the Forming Limit Curve (FLC), preserving its convexity, the separation between the deformation branches and the evolution of the limiting strains along the different loading paths. A systematic tendency toward underestimation of the FLC is observed for materials with high ductility, characterized by high UE·n values, while slight overestimation occurs for combinations with higher mechanical strength and lower strain redistribution capability. This behavior reflects the physical balance between strain hardening and strain localization. More ductile materials can redistribute stresses for longer before necking, whereas stronger materials with lower strain-hardening capacity tend to localize deformation earlier. Since the highest data density is concentrated in the intermediate region of the property space, the extremes of this domain are naturally more difficult to model with absolute accuracy.

These results demonstrate that model performance depends not only on mathematical approximation capability, but also on the interaction between data distribution, property-space complexity, and the physical mechanisms governing plastic instability. In this context, tree-based ensemble methods proved particularly suitable for capturing nonlinear relationships and variable interactions while maintaining high statistical stability.

Conclusions

This work demonstrated that Artificial Intelligence techniques can accurately predict the Forming Limit Curve (FLC) of Dual Phase steels using only uniaxial tensile properties, substantially reducing the need for extensive experimental testing. The construction of a physics-guided synthetic database, validated through Kolmogorov–Smirnov tests, ECDF analyses, and PCA projections, ensured the preservation of real data distributions and essential metallurgical correlations, providing a robust foundation for model training.

Among the evaluated techniques, tree-based models exhibited superior performance. Random Forest was the most robust and accurate model (MAE = 0.0052; MSE = 0.00011; $R^2 = 0.943$), closely followed by XGBoost. Both methods faithfully captured the geometry of the FLC across different strain paths and exhibited lower variability in prediction errors. The Neural Network, although capable

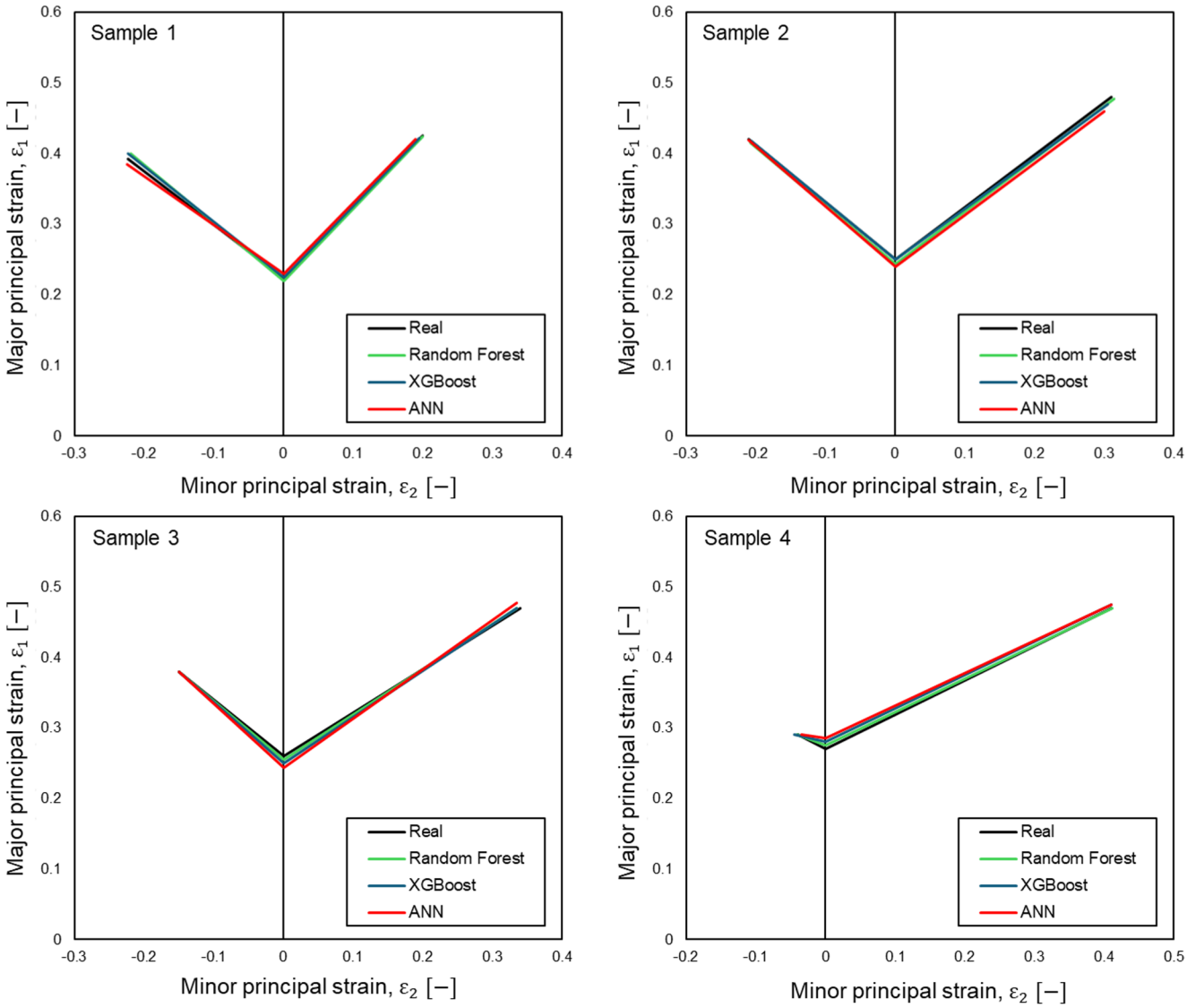

Fig. 14 Examples of FLCs from the inference test set [18]

of reproducing the overall curve shape, presented greater dispersion and reduced generalization capacity due to the limited amount of available data.

The results confirm that the combination of physics-guided descriptors, statistically controlled synthetic data generation, and ensemble models constitutes an efficient, reproducible, and physically coherent strategy for modeling the forming limits of AHSS steels. The proposed methodology can be incorporated into industrial stamping-process design workflows, accelerating the evaluation of new materials. Future perspectives include extending the framework to other AHSS classes, incorporating microstructural information, and adopting methods capable of quantifying predictive uncertainties.

Acknowledgements The authors thank CNPq, CAPES and FAPERGS for financial support.

Author contributions A.R. and P.D.D. wrote the main manuscript text and prepared all figures. R.M. and L.S. were responsible for the critical review and provided substantial revisions to improve the technical content and clarity. All authors read and approved the final manuscript.

Funding The Article Processing Charge (APC) for the publication of this research was funded by the Coordenação de Aperfeiçoamento de Pessoal de Nível Superior - Brasil (CAPES) (ROR identifier: 00x0ma614).

Data availability The datasets generated and/or analyzed during the current study are available from the corresponding author on reasonable request.

Declarations

Competing interests The authors declare no competing interests.

References

1. Rosiak A, Wermuth DP, Costa LLL (2025) Aços avançados de alta resistência: fundamentos e aplicações. Metal Forming – Technology and Innovation, Porto Alegre
2. Fonstein F (2017) Dual-phase steels. In: Fonstein F (ed) Automotive steels. Elsevier, Amsterdam, p 169–216
3. Chen HC, Cheng GH (1989) Effect of martensite strength on the tensile strength of dual-phase steels. J Mater Sci 24:1991–1994
4. Zhang J et al (2015) Effect of martensite morphology and volume fraction on strain hardening and fracture behavior of martensite–ferrite dual-phase steel. Mater Sci Eng A 627:230–240
5. Ahmad E et al (2012) Effect of martensite morphology on tensile deformation of dual-phase steel. J Mater Eng Perform 21:382–387
6. Wang J et al (2022) Effect of martensite morphology and volume fraction on the low-temperature impact toughness of dual-phase steels. Mater Sci Eng A. https://doi.org/10.1016/j.msea.2021.142424
7. Isik K et al (2014) Formability limits by fracture in sheet metal forming. J Mater Process Technol 214:1557–1565
8. Lou Y et al (2012) New ductile fracture criterion for prediction of fracture forming limit diagrams of sheet metals. Int J Solids Struct 49:3605–3615
9. Silva MB et al (2015) Fracture loci in sheet metal forming: a review. Acta Metallurgica Sinica (English Letters) 28:1415–1425
10. Elangovan K, Narayanan CS, Narayanasamy R (2010) Modelling of forming limit diagram of perforated commercial pure aluminium sheets using artificial neural network. Comput Mater Sci 47:1072–1078
11. Jaremenko C et al (2019) Determination of forming limits in sheet metal forming using deep learning. Materials. https://doi.org/10.3390/ma12071051
12. Thamm A et al (2023) Unsupervised deep learning for advanced forming limit analysis in sheet metal: a tensile test-based approach. Materials 16
13. Kotkunde N, Deole AD, Gupta AK (2014) Prediction of forming limit diagram for Ti-6Al-4V alloy using artificial neural network. Procedia Mater Sci 6:341–346
14. Dengiz CG, Şahin F (2023) Prediction of forming limit diagrams for steel sheets with an artificial neural network and comparison with empirical and theoretical models. Research on Engineering Structures and Materials
15. Derogar A, Djavanroodi F (2011) Artificial neural network modeling of forming limit diagram. Mater Manuf Process 26:1415–1422
16. Cheda AM et al (2019) Prediction of forming limit diagrams using machine learning. IOP Conference Series: Materials Science and Engineering 651:012107
17. Finamor FP, Wolff MA, Lage VS (2021) Prediction of forming limit diagrams from tensile tests of automotive grade steels by a machine learning approach. IOP Conference Series: Materials Science and Engineering 1157:012080
18. Demeri MY (1981) The formability of a dual-phase steel. Metall Trans A 12A:1181–1187
19. Marrapu B et al (2020) Experimental and numerical analysis on dual phase steel (DP780) sheet forming limit and effect of microstructure evolution on formability. J Mater Eng Perform 29:8247–8260
20. Konieczny AA (2001) On formability assessment of the automotive dual-phase steels. SAE Technical Paper 2001-01-3075. SAE International
21. Jeong Y, Panich S (2018) Forming limits of dual phase steels using crystal plasticity in conjunction with MK approach. Procedia Manuf 15:1816–1824
22. Alipour M et al (2021) Finite element and experimental method for analyzing the effects of martensite morphologies on the formability of DP steels. Mech Based Des Struct Mach 49:803–824
23. Ma B, Liu ZG, Jiang Z, Wu X, Diao K, Wan M (2016) Prediction of forming limit in DP590 steel sheet forming: an extended fracture criterion. Mater Des 96:401–408
24. Lu W et al (2024) A lightweight kernel density estimation and adaptive synthetic sampling method for fault diagnosis of rotating machinery with imbalanced data. Appl Sci. https://doi.org/10.3390/app142411910
25. Plesovskaya E, Ivanov S (2021) An empirical analysis of KDE-based generative models on small datasets. Procedia Comput Sci 193:442–452
26. Elreedy D, Atiya AF, Kamalov F (2024) A theoretical distribution analysis of SMOTE for imbalanced learning. Mach Learn 113:4903–4923
27. Dandekar A, Zen RAM, Bressan S (2018) A comparative study of synthetic dataset generation techniques. Hartmann S, Ma H, Hameurlain A, Pernul G, Wagner RR (eds). Database and Expert Systems Applications (DEXA 2018), Lecture Notes in Computer Science, vol 11030. Springer, p 387–395
28. Restrepo JP et al (2023) Nonparametric generation of synthetic data using copulas. Electronics. https://doi.org/10.3390/electronics12071601
29. Dankar FK, Ibrahim M (2021) Fake it till you make it: guidelines for effective synthetic data generation. Appl Sci 11:2158
30. Liu Y, Wang Y, Zhang J (2012) Random forest learning algorithm. Liu B, Ma M, Chang J (eds). Information Computing and Applications (ICICA 2012), Lecture Notes in Computer Science, vol 7473. Springer, p 246–252
31. Reis I, Baron D, Shahaf S (2019) Probabilistic random forest: a machine learning algorithm for noisy data sets. Astron J 157
32. Safhi AM, Dabiri H, Soliman A, Khayat KH (2023) Prediction of self-consolidating concrete properties using XGBoost machine learning algorithm: part 1 – workability. Constr Build Mater 408
33. Rocha RP, Riffel MH, Rosiak A, Follé LF, Lima TN, Schaeffer L (2025) Artificial intelligence-based modeling of hot deformation behavior in AA 5052-H32 alloy. The International Journal of Advanced Manufacturing Technology
34. Rosiak A, Schmeling M, Marcelino R, Schaeffer L (2024) Machine learning applied to predict the flow curve of steel alloys. Int J Adv Manuf Technol. https://doi.org/10.1007/s00170-024-14472-0
35. Diehl PD, Rosiak A, Marcelino R, Schaeffer L (2025) Predictive modeling of hardness in bainitic steel forging processes using artificial intelligence. Int J Adv Manuf Technol. https://doi.org/10.1007/s00170-025-16888-8

36. Shen F, Münstermann S, Lian J (2021) Forming limit prediction by the Marciniak–Kuczynski model coupled with the evolving non-associated Hill48 plasticity model. J Mater Process Technol. https://doi.org/10.1016/j.jmatprotec.2019.116384
37. Banabic D et al (2021) Developments of the Marciniak–Kuczynski model for sheet metal formability: a review. J Mater Process Technol. https://doi.org/10.1016/j.jmatprotec.2019.116446
38. Wang H, Wang Z (2023) Theoretical forming limit diagram based on induced stress in the thickness direction. Metals 13:456
39. Rault D (1976) Description of the deep-drawing end connected problems. In: Baudelet B (ed) Metal forming of the metals and alloys. CNRS, Paris, p 297–303